PHYSICAL REVIEW E **92**, 050601(R) (2015)

Nanoscale engineering of two-dimensional disordered hyperuniform block-copolymer assemblies

Gianluigi Zito,[1,*] Giulia Rusciano,[1] Giuseppe Pesce,[1] Anna Malafronte,[1] Rocco Di Girolamo,[1] Giovanni Ausanio,[1,2] Antonio Vecchione,[3,4] and Antonio Sasso[1]

[1]*Università degli Studi di Napoli Federico II, via Cintia I-80126 Napoli, Italy*

[2]*Consiglio Nazionale delle Ricerche–SPIN, via Cintia I-80126 Napoli, Italy*

[3]*Università degli Studi di Salerno, via Giovanni Paolo II 132, 84084 Fisciano (Sa), Italy*

[4]*Consiglio Nazionale delle Ricerche–SPIN U.O.S Salerno, via Giovanni Paolo II 132, 84084 Fisciano (Sa), Italy*

(Received 5 August 2015; published 10 November 2015)

Disordered hyperuniform (DH) media have been recognized as a new state of disordered matter that broadens our vision of material engineering. Here, long-range correlated disordered two-dimensional patterns are fabricated by self-assembling of spherical diblock-copolymer (BCP) micelles. Control of the self-assembling parameters leads to the formation of DH patterns of micelles that can host nanoscale material inclusions, therefore providing an effective strategy for fabricating multimaterial DH structures at molecular scale. Centroidal patterns are accurately determined by virtue of BCP micelles loaded with metal nanoparticles. Our analysis reveals the signature of nearly ideal DH BCP assemblies in the local density fluctuation and a dominant linear scaling in the local number fluctuation.

DOI: 10.1103/PhysRevE.92.050601 PACS number(s): 82.35.Jk, 61.20.Qg, 05.65.+b, 82.70.Dd

In the last decade, the study of local density fluctuations in many-body systems and general point patterns of particles has revealed the emergence, under particular conditions, of quasi-long-range correlated states even in disordered patterns, a property termed as hyperuniform disorder [1–6]. Disordered hyperuniform (DH) systems can be regarded as a new state of disordered matter. They possess statistically isotropic structures with no Bragg peaks, like liquids and glasses, but also a subtle, inherent order on the large length scale. Examples include maximally random jammed packings [3,7] and other systems [5,6,8–19].

A hyperuniform configuration is characterized by an observed number variance σ_N^2 that scales more slowly than the observation window volume $\tau \propto R^n$ in a n-dimensional space, where R is the window radius [2,20]. For a two-dimensional, uncorrelated Poisson process $\sigma_N^2 \propto R^2$, whereas for a hyperuniform configuration σ_N^2 ideally scales as R (namely, R^{n-1} for $n = 2$) [21]. Suppression of large-scale density fluctuations is also evident in the reciprocal space from the asymptotic small-$\mathbf{q}$ behavior of the isotropic structure factor $S(\mathbf{q})$ ($\mathbf{q} = q$) [21]. If the structure factor $S(q) \sim q$ for $q \to 0$, then $\sigma_N^2 \sim (b \ln R + c)R^{n-1}$, being b and c constants of the order of unity [5]. Similarly, a system with interparticle spacing D can be characterized by the local density variance

$$\sigma_\tau^2(r) = \langle \rho(r)^2 \rangle - \langle \rho(r) \rangle^2 \propto r^{-\lambda}, \tag{1}$$

where $\rho(r)$ is the number of particles in some observation window of normalized radius $r = R/D$ divided by the window volume $\tau(r)$ [9]. While for a Poisson point process $\lambda = n$, in a hyperuniform configuration density fluctuations are suppressed more efficiently, i.e., $\lambda > n$ [9].

Recently, so-called stealthy DH photonic band gap structures with unconventional properties have been demonstrated [21,22]. Novel thermodynamic and physical properties arise in DH systems and a new mechanic statistics has been introduced to explore their physics [6]. Thus far, however, controlling the fabrication process for applications and experiments at the nanoscale has remained elusive.

Here we propose a strategy based on chemical synthesis that allows fabricating a two-dimensional nanocolloidal film showing a hyperuniform disorder. Importantly, the nanoscale patterning process, based on block copolymer (BCP) self-assembling, has the potential of multimaterial structuring templated by the BCP morphology, thus providing a key for studying the properties of DH states in different materials (photonic, magnetic, plasmonic ones, etc.).

In a recent paper, we reported on an anomalous spot-to-spot variance of the plasmon-enhanced Raman scattering measured onto a BCP-templated nanostructure, which was ascribed to the excellent homogeneity of our disordered nanoisland pattern [18]. Here, we analyze the density fluctuation scaling of several patterns produced with the same protocol demonstrating the emergence of DH configurations. Figure 1 shows a schematic approach to this kind of nanostructuring. Our system consisted of inverse micelles of diblock copolymers of polystyrene-*block*-poly-4-vinylpyridine (PS-*b*-P4VP, 10,400-*b*-19,200 w/w, polydispersity index 1.27, Polymer Source Inc.). A solution of tetrahydrofuran (THF) and toluene (ratio 0.67 w/w) was used to induce the micelles formation by adding 97.2 mg of PS-*b*-P4VP in 20 ml of solvent (giving a relative concentration $c = 0.55\%$ w/w) after stirring at 700 rpm for 3 h at 25 °C, then for 2 h at 67 °C. Further details can be found in [18]. Neat micelles solutions were characterized by dynamic light scattering (DLS) and small angle x-ray scattering. A value of polydispersity of approximately 8% was initially measured by DLS for the solution of BCP micelles. Then, solutions of 2 ml were centrifuged at 15 krpm for 1 h in order to filter out unwanted material and reducing the system polydispersity by drawing desired amounts of liquid (typically 10^2 μl) at a designated height. A narrow diameter distribution with average $d = 37.2 \pm 0.5$ nm was found (spherical parameter 0.73 against 0.75 for ideal spheres), corresponding to a reduced polydispersity of $\simeq 1\%$.

Generally speaking, the soft BCP micelles can be deposited by spin coating or dip coating onto a supporting substrate (a commercial glass or a silicon wafer). Initially, the micelles

*zito@fisica.unina.it

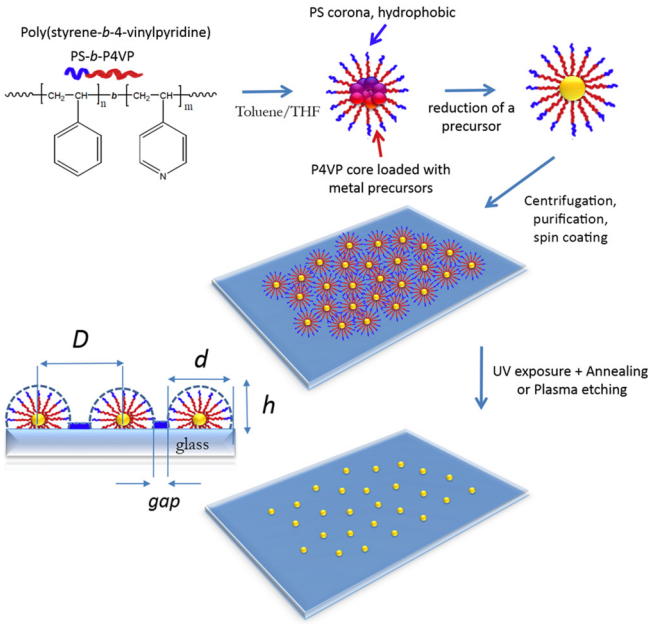

FIG. 1. (Color online) Scheme of the nanopatterning directed by BCP self-assembling upon fast solvent evaporation. BCP micelles can be loaded with many kinds of materials [23–25]. In this study, we used AgNPs and AuNPs. Metal nanoparticles can also be used to mark the BCP centroids pattern in order to avoid identification issues.

form a random colloidal system in Brownian motion and with no long-range correlation in solution. The self-assembling monolayer (SAM) is produced by the fast evaporation of the solvent during deposition [26]. When the solvent thickness becomes comparable to the micellar size, only displacements in the film plane are allowed. Then, micelles eventually freeze on the surface. Usually, micelles self-organize into a hexagonal two-dimensional colloidal crystal at equilibrium [23,27–30]. In particular, while solvent evaporation may freeze nonequilibrium configurations, THF solvent annealing of the deposited film produces equilibrium states characterized by hexagonal packings. Before solvent annealing, the actual degree or order depends on several parameters: initial concentration of the micelles, coating speed (solvent evaporation rate), surface wettability, temperature of deposition, and capillary forces in the solvent [31]. The formation of ordered arrays of nanoparticles can be seen as a delicate balance between attractive capillary forces between neighboring nanoparticles in the liquid film and repulsive forces due to electrostatic and steric interactions.

The micellar spacing can be regulated by varying the chain lengths of the copolymers, i.e., corona (PS) and core (P4VP) sizes, which determine the micelle diameter d (Fig. 1). On the other hand, for fixed BCP molecular weight ratio, the actual pattern can be altered by varying spin-coating speed v or initial concentration c, both influencing the interparticle distance D. Increasing concentration and decreasing (increasing) spin-coating (dip-coating) speed produce equivalent effects [28,31,32]. The maximum thickness h of the wetting film can be correlated to the capillary number $C = \gamma v/\Sigma$ (<1 in our case), thus to the surface tension Σ between solution and substrate and to the dynamic viscosity γ and density ρ of the wetting liquid by the following equation:

$$h \propto \sqrt{\frac{\Sigma}{\rho g}} C^{2/3} \propto v^{2/3}, \tag{2}$$

where g corresponds to the gravity acceleration. For a monolayer film, this means that the intermicelle distance goes like $\sim v^{1/3}$ (decreasing gap for increasing dip-coating speed; the opposite is true for spin-coating) [31]. Notably, the colloids assemble into a well ordered array in a certain range of deposition parameters $v_1 < v < v_2$, for which Eq. (2) holds [28,33]. It is worth mentioning that the number density of micelles achieved into the spin-coated film cannot be inferred from the number density of micelles in solution (given by the aggregation number of the micellar BCP) because other parameters are relevant for the micellar spacing, such as spin-coating velocity and surface wettability (in addition, most of the liquid is lost during spin coating). Commonly, a deformation of the array can be observed when the interparticle distance becomes comparable to the contact distance, $D = d$, therefore BCP micelles can be found in contact in a jammed disordered packing with no discernible gaps between them. For $v \leqslant v_1$ (spin-coating case), D becomes independent from v and a multilayer film starts to form. Typically, for nanotechnology applications that require highly ordered assemblies, solvent annealing is used to restore a crystalline hexagonal close-packed (hcp) structure [27,30]. The point is that varying the deposition velocity v provides a simple method for increasing the occupied volume fraction up to saturation, i.e., close to the formation of a two-layer film. We focused our attention on the isotropic disordered assembly generated at this limit packing, demonstrating that the array deformation is accompanied to a very homogenous density and hyperuniform quasi-long-range correlations.

As previously mentioned, the occupied volume fraction may be also increased by virtue of a larger initial concentration of micelles in solution. We used spin-coating velocities v in the range 0.5–6.0 krpm, but we found poorly reproducible coatings (on the large area) for spin-coating speeds <1 krpm—necessary to approach the contact spacing $D = d$. Therefore, we adopted a concentration c proximal to a second layer formation to maximize the filling fraction of the close-packed monolayer [28], from now on indicated as saturated BCP SAM. After inspecting the deposited films by scanning and/or transmission electron microscopies (SEM/TEM) or atomic force microscopy (AFM), we found an interesting condition of dense homogeneous SAM for $c = 0.77\%$ w/w. A representative AFM map (tapping mode) of this BCP pattern is shown in Fig. 2(a). The film revealed a highly regular lattice with an average height of the nanofeatures of $h \simeq 13.6$ nm (as accessible to the tip), presumably corresponding to bumps' morphology over a bottom PS layer according to previous studies [18,28], which also denoted BCP micelles slightly deformed upon contact with the surrounding micelles.

Then we imposed a similar condition for micelles loaded with metal nanoparticles (NPs) produced by *in situ* reduction of a metal precursor. In particular, in our case, micelles were loaded by complexing the P4VP core either with Ag^+, from 203.7 mg of $AgNO_3$ in 20 ml of solvent, or with Au^{3+}, from 470 mg of $HAuCl_4 \cdot 3H_2O$, both corresponding to a

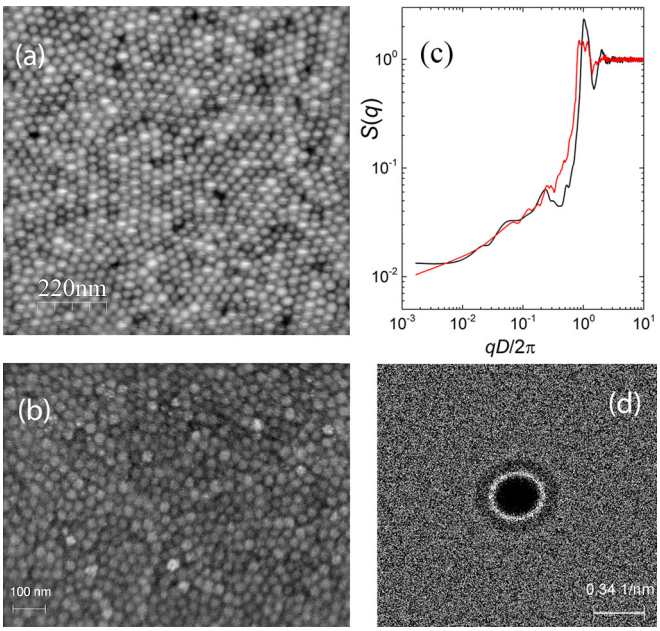

FIG. 2. (Color online) (a) Representative AFM topography map of a film of bare BCP micelles produced at $c = 0.77\%$ w/w and $v = 1$ krpm on a silicon wafer: only short-range topological order is observed after deformation of the hexagonal array. (b) SEM micrograph of an analogous film of BCP micelles loaded with AgNPs. (c) Azimuthally averaged static structure factors: the black line corresponds to the bare BCP micelles pattern shown in (a); the red line corresponds to the azimuthal average of the structure factor map shown in (d) and is relative to a single pattern of BCP micelles marked with AuNPs of approximately 5 nm: a nearly linear behavior is evident for $q \to 0$; extrapolated $S(0) \simeq 0.008$. The NPs allowed individuating experimentally the centroidal pattern.

concentration of 0.55% w/w of BCP in solution. All chemicals for NP synthesis were purchased from Sigma Aldrich. During the loading procedure, metal ions accumulate into the P4VP core, negatively charged above the isoelectric point (pH = 8.3). $NaBH_4$ was used to reduce the core-loaded ions to metal nanoparticles [18,34]. Finally, our metal-BCP solution was centrifuged at 11 krpm for 20 min to separate possible unloaded supernatant micelles, which filtered out unwanted material and left more concentrated solution of nanocomposite micelles, passing from 0.55% to 0.77% w/w, thus providing an increase of the occupied volume fraction in the deposited film. A 100 μl volume of solution was left over the supporting glass for 30 s before starting the spin coating at 1.0-krpm speed for 60 s, in controlled ambient atmosphere. An extremely uniform SAM was achieved.

In the case of AgNP clusters filling the BCP core, the pattern was characterized by metal islands gaps <5 nm, i.e., below the intercore distance of $\simeq 10$ nm imposed by the PS shells of the initial micelles, probably because of partial unfolding of polystyrene [18,28], which is a direct consequence of the soft nature of the BCP system and its capability to accommodate structural variations. The degree of order was little affected by the presence of nanoparticles [Fig. 2(b)], as discussed later.

We used monocrystalline silicon wafer [100] (STMicroelectronics, Switzerland) of 20×20 mm^2 as supporting substrate for AFM analysis, and also standard borosilicate glass coverslips (ThermoScientific, USA) and ITO-coated glass coverslips (JEOL Ltd., Italy) of 24×24 mm^2 for TEM and SEM analysis, respectively. As pretreatment, coverslips were soaked in an ultrasonic bath (UB) for 22 min at 60 °C in acetone and then in Milli-Q water solution with sonic bath soap (3% w/w), then rinsed first with Milli-Q water in UB, and then again with propanol-2 (same procedure). Silicon wafers were similarly sonicated in ethanol. Then, all samples were dried with a nitrogen pump.

Finally, we studied the density fluctuations of the configurations achieved. The centroids and morphological information of the bare micelles were identified by taking advantage of atomic force microscopy (NanoScope, Digital Instruments). The system was equipped with an ultrasharp etched silicon tip with curvature radius of ~ 5 nm operating in tapping mode (frequency $\simeq 300$ kHz). The inspected patterns were chosen from the central region of the samples and had a typical size of a few microns in order to ensure sufficient resolution in the determination of the configurations of micelles and for including, at the same time, a statistically significant number of nanoparticles for the analysis. As for instance, in a topographic or phase map of 512 pixels over an area of 1.34 μm of width, the achieved spatial resolution was $\Delta x \simeq 2.6$ nm and included about 10^3 nanoparticles, therefore allowing acquiring the relevant morphological information of a micelle having a diameter of 37 nm ($d/\Delta x \simeq 14$). Typically, the analyzed patterns included a number of particles in the range 1000–3000 [35]. The acquired images were also processed using a Voronoi-Delaunay triangulation algorithm. In addition, metal-loaded micelles allowed identifying experimentally the centroids pattern by marking the centers of the micelles. In fact, once the polymer is removed by UV exposure (254 nm) [18], thermal annealing allowed inducing the coalescence of clusters of NPs to single nanoparticles at the micellar centers [34]. This expedient allows minimizing artifacts that become relevant when BCP micelles are in contact. Similar results were achieved also by oxygen plasma etching. Examples of so-obtained metal NP patterns can be found in Refs. [24,28,31,34,36,37]. A preliminary indication of the achievement of a DH configuration in our pattern was found in the azimuthally averaged structure factor of a metal-loaded BCP SAM (red line) [Figs. 2(c) and 2(d)]. Indeed, we observed a nearly linear behavior for $q \to 0$. However, the structure factor remained finite at $q = 0$, with typical values $S(0) \simeq 10^{-2}$; in addition, deviations from linearity were evident for low q values [Fig. 2(c)]. Such deviations were also more pronounced for the structure factor of the bare BCP micelles pattern (black line) [Fig. 2(c)]. Then, in order to assess whether such behavior was affected by the finite size of the examined patterns or by the polydispersity of the system, which are known to reduce the capability of detecting hyperuniformity, we studied both the local number and density fluctuation scaling as a function of the radius R of the sampling circular window, normalized to the interparticle distance D. This was done from a minimum radius equal to the average interparticle distance D up to the maximum length $L/2$ imposed by the size of the experimental pattern. Smaller patterns were replicated in a 3×3 matrix in a stitching image to include boundary centroids in the analysis, which simulated periodic boundary conditions of supercell approximation method. The outcomes

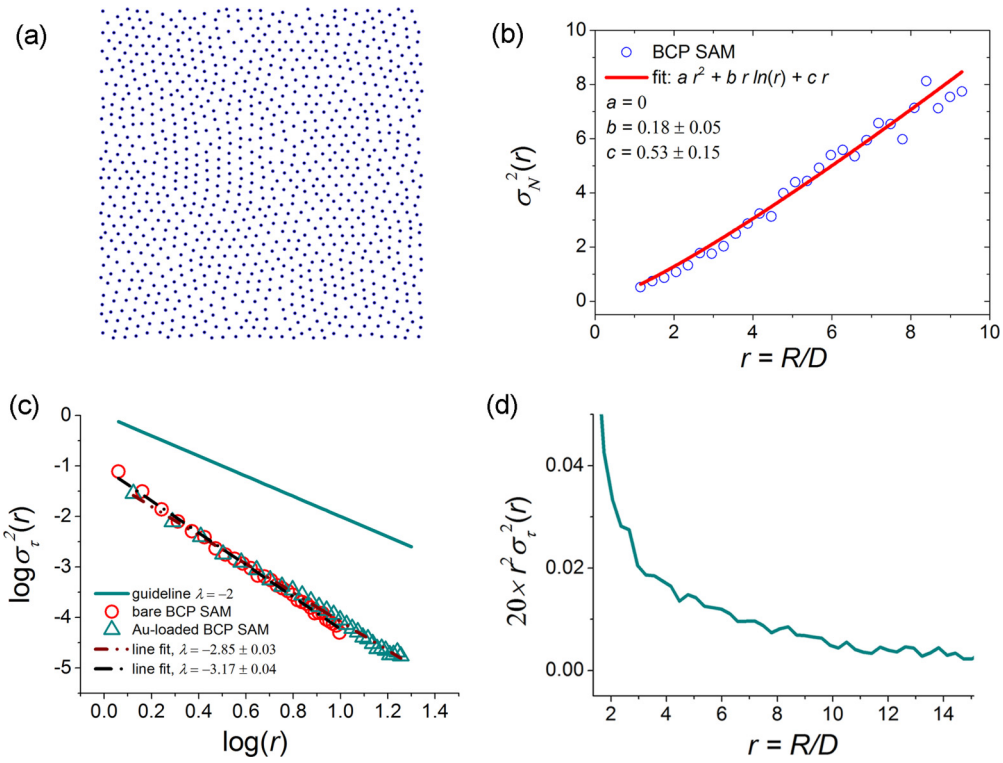

FIG. 3. (Color online) (a) Centroidal pattern of unloaded BCP SAM at saturation (width = 1340 nm, number of particles $\simeq$ 1000). (b) Local number variance of unloaded BCP SAM as a function of the sampling window radius: the fit shows a dominant linear scaling. (c) Local density variance as a function of the sampling window radius for a BCP SAM of bare micelles and metal-loaded micelles: the exponents of scaling point out a nearly ideal DH configuration ($\lambda \simeq -3$); a standard disorder scaling, $\lambda = -2$, is also depicted for comparison; our analysis is summarized in Table I. (d) The figure of merit $r^2\sigma_\tau^2(r)$ shows a nonconstant behavior, again a signature of a DH state.

of the analysis in these cases were not affected by such a procedure, which allowed increasing the accuracy of the obtained fit values. For each radius, a distribution of point numbers and related statistics were collected by centering the sampling disk on each point of the pattern [5]. Figure 3(a) shows a representative centroidal pattern obtained from a saturated BCP SAM of unloaded micelles. The result of the number fluctuation analysis is shown in Fig. 3(b). The data were fitted to the following model:

$$\sigma_N^2(r) = ar^2 + br\ln(r) + cr, \tag{3}$$

with $r = R/D$ and $a,b,c \geqslant 0$ in order to elicit the relevant asymptotic scaling [5]. Data associated to the drop-off of the experimental data for $R \simeq L/2$ (finite window artifact) were removed from the fit [20]. The suppression of the quadratic term in the fit and the dominant surface-term scaling $c > b$ provide remarkable proof of the emergence of a hyperuniform disorder. In particular, we found a coefficient $a \simeq 10^{-9}$. For the sake of simplicity, from now on we pose values $\ll 1$ equal to zero, and as such we write $a = 0$ for fit values $< 10^{-8}$ (the same holds for b and c). The fit values were influenced by the extent of the pattern because of the drop-off of the experimental data for $R \simeq L/2$. The precise values indicated in Fig. 3(b) are the result of a particular fit. More accurate estimates of the actual indetermination of the fit parameters can be found in Table I, where the half-ranges of estimated values are used as experimental errors. The quadratic term suppression was repeatedly verified with comparable $\{b,c\}$ coefficients on a set of regions of the pattern giving $b \simeq 0.0$–0.3 and $c \simeq 0.5$–1.1, and also for metal-loaded BCP micelles (see Table I). Interestingly, we verified the scaling to be purely quadratic for a nonsaturated disordered pattern produced at a larger spin-coating speed of 3 krpm (Table I).

While local number variance was readily determined from the experimental centroids or AFM analysis, estimating the volume fraction actually reached was particularly difficult because the soft BCP appeared deformed in a sort of compressed, jammed state [Fig. 2(a)] [7,20]. Then, we studied the scaling of the density fluctuations [Eq. (1)] fitted to the power law $\sigma_\tau^2(r) = \alpha r^\lambda$ ($r = R/D$), where the exponent λ is now intended as a free parameter of the fit. The $\sigma_\tau^2(r)$ fluctuation corresponding to the number variance shown in Fig. 3(b) is given in Fig. 3(c) together with the case of a BCP SAM of metal-loaded micelles at saturation. The power law exponents resulting from the fit point out a hyperuniform disorder configuration [9,20]. In Fig. 3(d) we also plot the corresponding figure of merit $r^2\sigma_\tau^2(r)$, which shows the typical nonconstant scaling of a DH pattern [20] (see also Table I). Given the algorithm dependency, we carried out the same analysis for a set of two-dimensional patterns to provide a comparison of the scaling behaviors, in particular for a random Poisson pattern, a hexagonal close-packed crystal, a decagonal quasicrystal, and an ideal disordered hyperuniform pattern extracted from Ref. [6] (Table I). Also more exotic patterns were analyzed [38,39]. The comparison showed that all DH states were efficiently individuated and included saturated BCP SAM patterns.

TABLE I. Fit values a, b, c (local number variance), and λ (local density variance) for (i) random Poisson point process; (ii) nonsaturated BCP SAM, $v = 3$ krpm; (iii) saturated BCP SAM ($c = 0.77\%, v = 1$ krpm); (iv) metal-loaded BCP SAM at saturation ($c = 0.77\%, v = 1$ krpm); (v) average metal-loaded BCP SAM at saturation ($c = 0.77\%, v = 1$ krpm); (vi) hexagonal close-packed crystal (hcp); (vii) decagonal quasicrystal (QC); and (viii) ideal DH state from Ref. [6]. Constant = c; nonconstant = nc.

Pattern type	a	b	c	λ	$r^2\sigma_\tau^2(r)$
(i) Random Poisson	1.6 ± 0.1	0	0	-2.0 ± 0.1	c
(ii)[a] BCP SAM, nonsaturated	1.1 ± 0.2	0	0	-2.0 ± 0.2	c
(iii)[a] BCP SAM, saturated	0	0.15 ± 0.10	0.6 ± 0.2	-3.20 ± 0.15	nc
(iv)[a] BCP SAM, metal loaded	0	0.09 ± 0.05	1.0 ± 0.2	-2.95 ± 0.15	nc
(v)[a] BCP SAM, average	0	0.11 ± 0.08	1.1 ± 0.3	-2.8 ± 0.2	nc
(vi)[a] HCP	0	0	0.65 ± 0.05	-3.0 ± 0.2	nc
(vii) Decagonal QC	0	0	1.2 ± 0.2	-3.1 ± 0.2	nc
(viii) Ideal DH	0	0	0.7 ± 0.1	-3.2 ± 0.2	nc

[a]Experimental patterns.

In the recent years, it has been understood that polydispersity of spheres and disks does not prevent hyperuniform organization [7]. However, it may pose limits to the capability of detecting hyperuniformity, in particular when studying the structure factor, which neglects details of particle shapes and therefore is in general not sufficient to properly characterize the packings [7,40]. On the other hand, hyperuniformity can be detected efficiently by using the compressibility description [7] or the local-volume fraction description to account for the polydispersity of the system [20]. In addition, while reciprocal space approach requires large patterns, in the direct space, the significant length scale on which the relevant structural information (positions, diameters) must be acquired can be smaller ($L \gtrsim 10D$) [20]. In our case, we found that the number fluctuation analysis was sufficient to detect hyperuniformity. At this stage, we ascribe this circumstance to the limited polydispersity of our system ($\sim 1\%$) and to the higher accuracy of the direct-space analysis. It is also worth noticing that the soft nature of the micelles could be responsible for subtle mechanisms and a sort of structural "smoothing" of the particles configuration.

It is also important to notice that the inspected regions of the films did not show the same degree of hyperuniformity. The coefficient λ had a local character and was found to depend on the particular area inspected, probably because of experimental deviations from an ideal homogeneous interaction of the film with the substrate surface. The inspected patterns were only randomly sampled over an area of the film of the order of 100 mm^2 and had typical areas $<30\,\mu m^2$. We found an asymmetric distribution of values of λ in the range $(-3.2, -2.2)$, with an average around $\lambda = -2.8 \pm 0.2$ (see Table I). Such a variability could be ascribed to the interaction with the supporting substrate, but may also be the result of other mechanisms affecting the local character of the film density, such as the existence of a characteristic length scale of hyperuniformity as found in [9,19]. Therefore, a future challenge will be producing a pattern with accurate control of the hyperuniformity degree on the large area.

In conclusion, this study points out that self-assembling of soft BCP represents a possible route for fabricating disordered hyperuniform patterns under suitable conditions. The emergence of an isotropic hyperuniform configuration in a dense, random close packing of BCP micelles is likely due to the interplay between attractive capillary forces and repulsive electrostatic and steric interactions among micelles. Our analysis also demonstrates that hyperuniformity holds in the case of loaded BCP micelles. This result paves the way to the fabrication of DH patterns templated by BCP self-assembling. Several types of materials (Ag, Au, Pt, Co, CoPt, Fe_2O_3, FePt, ZnO, TiO_2, SiO_2, etc. [23,24]) may be loaded into BCP micelles, which provides a key for studying fundamental properties—such as energy transport and localization—in DH configurations of various materials. Loading nanocrystals into a BCP micelle is accomplished by coordinating precursor ions to the micellar cores by protonation. However, micelles can also attract electrostatically (or by proper functionalization) nanocrystals or biomolecules like DNA after deposition [24,25]. We used BCP micelles loaded with plasmonic nanoparticles of silver and gold. Gold nanoparticles are typically used to form biomolecular ligands (DNA, proteins, etc.). Therefore, patterns of AuNPs could be used to form DH patterns of biomolecules, as for instance for studying cell surface adsorption, recognition, or signaling in the case of disordered, correlated organization [41,42].

We acknowledge financial support from Ministero dell'Istruzione, dell'Università e della Ricerca of Italy, Grant No. FIRB 2012-RBFR12WAPY, and from University of Naples Federico II, Compagnia di San Paolo Istituto Banco di Napoli-Fondazione (STAR Project LARA).

[1] S. Torquato, T. M. Truskett, and P. G. Debenedetti, Phys. Rev. Lett. **84**, 2064 (2000).

[2] S. Torquato and F. H. Stillinger, Phys. Rev. E **68**, 041113 (2003).

[3] C. E. Zachary, Y. Jiao, and S. Torquato, Phys. Rev. Lett. **106**, 178001 (2011).

[4] Y. Jiao, F. H. Stillinger, and S. Torquato, Phys. Rev. E **81**, 041304 (2010).

[5] Y. Jiao, T. Lau, H. Hatzikirou, M. Meyer-Hermann, J. C. Corbo, and S. Torquato, Phys. Rev. E **89**, 022721 (2014).
[6] S. Torquato, G. Zhang, and F. H. Stillinger, Phys. Rev. X **5**, 021020 (2015).
[7] L. Berthier, P. Chaudhuri, C. Coulais, O. Dauchot, and P. Sollich, Phys. Rev. Lett. **106**, 120601 (2011).
[8] E. Tjhung and L. Berthier, Phys. Rev. Lett. **114**, 148301 (2015).
[9] D. Hexner and D. Levine, Phys. Rev. Lett. **114**, 110602 (2015).
[10] R. L. Jack, I. R. Thompson, and P. Sollich, Phys. Rev. Lett. **114**, 060601 (2015).
[11] R. Kurita and E. R. Weeks, Phys. Rev. E **84**, 030401 (2011).
[12] A. Gabrielli, B. Jancovici, M. Joyce, J. L. Lebowitz, L. Pietronero, and F. Sylos Labini, Phys. Rev. D **67**, 043506 (2003).
[13] L. Reatto and G. V. Chester, Phys. Rev. **155**, 88 (1967).
[14] D. Levesque, J.-J. Weis, and J. Lebowitz, J. Stat. Phys. **100**, 209 (2000).
[15] A. Scardicchio, C. E. Zachary, and S. Torquato, Phys. Rev. E **79**, 041108 (2009).
[16] R. D. Batten, F. H. Stillinger, and S. Torquato, J. Appl. Phys. **104**, 033504 (2008).
[17] C. de Rosa, F. Auriemma, C. Diletto, R. D. Di Girolamo, A. Malafronte, P. Morvillo, G. Zito, G. Rusciano, G. Pesce, and A. Sasso, Phys. Chem. Chem. Phys. **17**, 8061 (2015).
[18] G. Zito, G. Rusciano, G. Pesce, A. Dochshanov, and A. Sasso, Nanoscale **7**, 8593 (2015).
[19] J. H. Weijs, R. Jeanneret, R. Dreyfus, and D. Bartolo, Phys. Rev. Lett. **115**, 108301 (2015).
[20] R. Dreyfus, Y. Xu, T. Still, L. A. Hough, A. G. Yodh, and S. Torquato, Phys. Rev. E **91**, 012302 (2015).
[21] M. Florescu, S. Torquato, and P. J. Steinhardt, Proc. Natl. Acad. Scie. USA **106**, 20658 (2009).
[22] W. Man, M. Florescu, K. Matsuyama, P. Yadak, G. Nahal, S. Hashemizad, E. Williamson, P. Steinhardt, S. Torquato, and P. Chaikin, Opt. Express **21**, 19972 (2013).
[23] C. Park, J. Yoon, and E. L. Thomas, Polymer **44**, 6725 (2003).
[24] S. M. Taheri, S. Fischer, and S. Förster, Polymer **3**, 662 (2011).
[25] F. L. Yap, P. Thoniyot, S. Krishnan, and S. Krishnamoorthy, ACS Nano **6**, 2056 (2012).
[26] A. S. Dimitrov and K. Nagayama, Langmuir **12**, 1303 (1996).
[27] S.-H. Yun, S. il Yoo, J. C. Jung, W.-C. Zin, and B.-H. Sohn, Chem. Mater. **18**, 5646 (2006).
[28] S. Krishnamoorthy, R. Pugin, J. Brugger, H. Heinzelmann, and C. Hinderling, Adv. Funct. Mater. **16**, 1469 (2006).
[29] S. Krishnamoorthy, C. Hinderling, and H. Heinzelmann, Mater. Today **9**, 40 (2006).
[30] W. Lee, S. Lee, X. Zhang, O. Rabin, and R. Briber, Nanotechnology **24**, 045305 (2013).
[31] J. Bansmann, S. Kielbassa, H. Hoster, F. Weigl, H. G. Boyen, U. Wiedwald, P. Ziemann, and R. J. Behm, Langmuir **23**, 10150 (2007).
[32] S. Krishnamoorthy, K. K. Manipaddy, and F. L. Yap, Adv. Funct. Mater. **21**, 1102 (2011).
[33] B. Gorzolnik, Ph.D. thesis, RWTH Aachen University, Warsaw, 2007.
[34] S. K. Cha, J. H. Mun, T. Chang, S. Y. Kim, J. Y. Kim, H. M. Jin, J. Y. Lee, J. Shin, K. H. Kim, and S. O. Kim, ACS Nano **9**, 5536 (2015).
[35] An analogous compromise about spatial resolution and extent of the inspected area was taken into account for SEM analysis, but in that case particles were up to $\sim$5000.
[36] S. Fischer, A. Salcher, A. Kornowski, H. Weller, and S. Förster, Angew. Chem., Int. Ed. **50**, 7811 (2011).
[37] U. Wiedwald, L. Han, J. Biskupek, U. Kaiser, and P. Ziemann, Beilstein J. Nanotechnol. **1**, 24 (2010).
[38] O. U. Uche, F. H. Stillinger, and S. Torquato, Phys. Rev. E **70**, 046122 (2004).
[39] C. E. Zachary and S. Torquato, J. Stat. Mech.: Theory Exp. (2009) P12015.
[40] C. E. Zachary, Y. Jiao, and S. Torquato, Phys. Rev. E **83**, 051308 (2011).
[41] M. D. Mager, V. LaPointe, and M. M. Stevens, Nat. Chem. **3**, 582 (2011).
[42] R. L. Juliano, Ann. Rev. Pharmacol. Toxicol. **42**, 283 (2002).